crystals

MDPI

Article

Fast, Accurate and Full Extraction of Coupling-of-Modes Parameters by Finite Element Method

Xueping Sun [1], Rui Ma [2], Shun Zhou [1], Xiuting Shao [3], Jin Cheng [1], Dabin Lin [1], Wen Wang [4] and Weiguo Liu [1,*]

[1] School of Optoelectronic Engineering, Xi'an Technological University, Xi'an 710021, China; sunxueping.1988@163.com (X.S.); zsemail@126.com (S.Z.); 624788236@163.com (J.C.); dabinlin@xatu.edu.cn (D.L.)
[2] School of Microelectronics, Xidian University, Xi'an 710071, China; marui@xatu.edu.cn
[3] School of Information Science and Engineering, Shandong Normal University, Jinan 250358, China; shaoxiuting@126.com
[4] State Key Laboratory of Acoustics, Institute of Acoustics, Chinese Academy of Sciences, Beijing 100190, China; wangwenwq@mail.ioa.ac.cn
* Correspondence: wgliu@163.com

Abstract: This paper presents a new numerical approach for the full extraction of the coupling-of-modes (COM) parameters by stationary and eigenfrequency analyses in the finite element method (FEM). This is a fast method extracting from the results of static analysis and eigenfrequency analysis. It avoids the long calculation time of admittance frequency response analysis, which is commonly used in extracting COM parameters. In addition to the usual COM parameters (velocity, reflection coefficient, transduction coefficient and capacitance), the phases of reflection and transduction coefficient can be also extracted with this method. The proposed method was applied to different cutting types $LiNbO_3$ with different types of thicknesses in a varying interdigital transducer (IDT). These examples show that our approach has great potential in extracting all the COM parameters of the Rayleigh SAW for all kinds of IDT structures. Therefore, it is a fast, accurate, general and full extraction approach of COM parameters.

Keywords: surface acoustic wave; interdigital transducer; coupling-of-mode; finite element method

Citation: Sun, X.; Ma, R.; Zhou, S.; Shao, X.; Cheng, J.; Lin, D.; Wang, W.; Liu, W. Fast, Accurate and Full Extraction of Coupling-of-Modes Parameters by Finite Element Method. *Crystals* **2022**, *12*, 706. https://doi.org/10.3390/cryst12050706

Academic Editors: László Kovács and Alexei A. Bokov

Received: 3 April 2022
Accepted: 14 May 2022
Published: 16 May 2022

1. Introduction

The design of high-performance SAW devices requires accurate and efficient simulation techniques. The complexity of modeling IDT or functional gradient materials [1,2] make it difficult to obtain a rigorous analytical solution. FEM is an effective method in designing SAW devices because it can directly describe the coupled partial differential equations involving the electric and mechanical fields in a grating consisting of a piezoelectric substrate with electrodes [3]. It can handle arbitrary materials and crystal cuts, different electrode shapes and structures including multiple metal and dielectric layers [4,5]. Compared with phenomenological models, superior performances of FEM on accuracy have been validated when considering a necessary discretization of at least 10 elements per wavelength. That is to say, the accuracy depends on the number of grids. Consequently, it is time-consuming to simulate the whole device, since a huge number of grids are necessary to improve the precision, but which require intensive computation [6,7]. Therefore, it cannot be directly used to optimize the device performance.

Compared with other phenomenological models, such as the equivalent circuit model [8], the COM model is a more efficient model in simulating and designing SAW devices. In addition to the acoustoelectric interactions of the electric current with the surface acoustic waves, the COM model considers the excitation, propagation and mutual reflection of counter-propagating waves in a continuous medium [9]. Since it is a phenomenological

model, the heavy dependence of the COM model on the accurate COM parameters is evident. Many researchers have made much effort to acquire these parameters experimentally and theoretically. Hartmann et al. extracted the needed COM parameters from measurements [10,11]. However, this process is both time-consuming and expensive because of the many degrees of SAW structures, such as the relative electrode thickness, the metallization ratio and the electrode profile. Some numerical methods, such as a combination of FEM and boundary element methods [12,13], a full FEM [14] and finite element method–spectral domain analysis [15,16], have also been employed for COM parameters extraction.

Regarding to the reflection coefficient and transduction coefficient, most of researchers are got only in their absolute value. To obtain the best unidirectivity for SPUDT, one must know the accurate COM parameters, including the phases of reflection coefficient and transduction coefficient, to find out if the length between the transduction and reflection centers is 1/8 wavelength or not [17]. Hashimoto et al. used the input admittance to find the two resonances and two antiresonances to extract all the absolute values of the COM parameters except capacitance C and the phase difference between the phase of reflection coefficient and the double phase of the transduction coefficient [15,18,19]. They obtained capacitance C by the fitting methods, with the results of the input admittance calculated using the MSYNC software. However, the sign of the phase difference could not be determined. Yong'an Shui et al. used the periodic Green's function method to extract all the COM parameters, including the phase of reflection coefficient, but not the phase of transduction coefficient [20].

In this paper, we will demonstrate an approach to extract all the COM parameters. This approach makes full use of the results of static analysis and eigenfrequency analysis obtained by the FEM. It avoids the long calculation time in the frequency response analysis. Subsequently, we will demonstrate the results of several examples of its application. These results show that this approach is powerful to fully extract the COM parameters of the Rayleigh wave for all kinds of IDT structures on arbitrary materials.

2. Theory to Extract COM Parameters

2.1. COM Model

It is assumed that there are two counter-propagating waves which exist in a grating, where one of them propagates toward the $+x$ direction, whereas the other propagates toward the $-x$ direction. The two waves are represented as $R(x)$ and $S(x)$, respectively. There are three common types of COM differential equations. These differential equations vary depending on whether the direction of the current flow is the same or opposite to the coordinate system and the sign of reflection coefficient κ. As shown in Figure 1, $R(x)$ and $S(x)$ represent the two counter-propagating waves, and $I(x)$ is the current caused by the induced charges in the electrodes when the transducer is driven by a voltage V, whose direction is opposite to x. The drive voltage V and current I are defined by their half-power amplitude values.

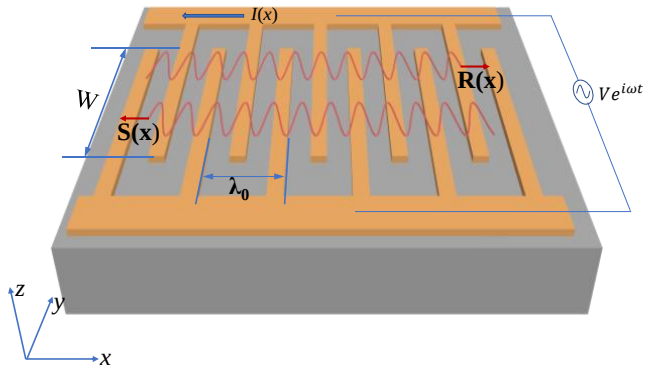

Figure 1. A SAW transducer.

Introducing the slow varying fields $R_0(x)$, $S_0(x)$ of $R(x)$ and $S(x)$:

$$\begin{cases} R(x) = R_0(x)\exp(-ik_0x) \\ S(x) = S_0(x)\exp(ik_0x) \end{cases}, \tag{1}$$

where $k_0 = 2\pi/\lambda_0$. Moreover, defining a detuning parameter Δ as:

$$\Delta = k - k_0 = \frac{\omega}{v} - \frac{2\pi}{\lambda_0}, \tag{2}$$

where ω is the angular frequency, v is the velocity and λ_0 is the electric period of the gratings. Then, the final COM equations can be written as [9,21]:

$$\begin{cases} \dfrac{\partial R_0}{\partial x} = -i\Delta R_0(x) + i\kappa S_0(x) + i\alpha V \\ \dfrac{\partial S_0}{\partial x} = -i\kappa^* R_0(x) + i\Delta S_0(x) - i\alpha^* V \\ \dfrac{\partial I}{\partial x} = -2i\alpha^* R_0(x) - 2i\alpha S_0(x) + i\omega C V \end{cases}, \tag{3}$$

where velocity v, the reflection coefficient κ, the transduction coefficient α and the static capacitance per unit length C are the four independent COM parameters to be determined. Generally, κ and α are complex numbers.

If we define the reflection coefficient $\kappa = -\kappa$, the resulting COM equations are the second form, which has been widely used in Japan [18,22,23]. If we define $I(x) = -I(x)$ and introduce the thin film resistance of an interdigital transducer, the third form COM equations would be derived. This form was also used in many papers [24–26].

No matter which kinds of COM model is used, all the four characteristic parameters need to be extracted. In the next section, we developed a parameters extraction technique for all four COM parameters mentioned above based on the FEM.

2.2. Extraction Technique of COM Parameters

The static capacitance is a measure of the electrostatic energy stored in an IDT and it can be calculated from the charge distribution and electric field distribution excited by the transducer subject to a constant voltage. When the applied voltage is 1V, the static capacitance of one period C_p is the integral of charge distribution on the electrode.

The other parameters can be extracted from the stopband characteristics of the short-circuited and open-circuited grating. For a short-circuited grating, the voltage will be set at 0V, and the COM equations will be reduced to the form [27] given in Equation (4).

$$\begin{cases} \dfrac{\partial R_0}{\partial x} = -i\Delta R_0(x) + i\kappa S_0(x) \\ \dfrac{\partial S_0}{\partial x} = -i\kappa^* R_0(x) + i\Delta S_0(x) \end{cases}, \tag{4}$$

The solution is of the form in Equation (5)

$$\begin{cases} R(x) = c_1\exp[-i(k_0 - q_{sc})x] + c_2\exp[-i(k_0 + q_{sc})x] \\ S(x) = \frac{1}{\kappa}\{c_1(\Delta + q_{sc})\exp[i(k_0 + q_{sc})x] + c_2(\Delta - q_{sc})\exp[i(k_0 - q_{sc})x]\} \end{cases}, \tag{5}$$

and satisfies the dispersion relation [18] in Equation (6):

$$q_{sc} = \begin{cases} -\sqrt{\Delta^2 - |\kappa|^2} & (\Delta < -|\kappa|) \\ -i\sqrt{|\kappa|^2 - \Delta^2} & (\Delta < |\kappa|) \\ -\sqrt{\Delta^2 - |\kappa|^2} & (\Delta > |\kappa|) \end{cases}, \tag{6}$$

where c_1 and c_2 are arbitrary coefficients of the two eigenmodes which are determined by the initial and boundary conditions. Each of them may be interpreted as combinations of an incident wave and a reflected wave. It can be seen from Equations (5) and (6) that the eigenmodes form a stopband in the frequency region, $|\Delta| < |\kappa|$. Here, we use the phase φ_κ and amplitude $|\kappa|$ to describe the reflection coefficient as $\kappa = |\kappa| \exp(i\varphi_\kappa)$. The amplitude of κ determines the width of the stopband. The lower and upper frequencies of the stopband f_{s+} and f_{s-} can be obtained by considering the zeros of the dispersion relation [28,29]. Then, we have:

$$\begin{cases} f_{s+} = \left(1 + \dfrac{|\kappa|\lambda_0}{2\pi}\right) f_s \\ f_{s-} = \left(1 - \dfrac{|\kappa|\lambda_0}{2\pi}\right) f_s \end{cases}, \tag{7}$$

From Equation (7), the center frequency of the short-circuited grating f_s and $|\kappa|$ can be represented as Equations (8) and (9).

$$f_s = \frac{f_{s+} + f_{s-}}{2}, \tag{8}$$

$$|\kappa| = \frac{2\pi}{\lambda_0} \frac{f_{s+} - f_{s-}}{f_{s+} + f_{s-}}, \tag{9}$$

The Rayleigh mode effective velocity v in a short-circuited grating can be calculated using the following equation:

$$v = f_s \lambda_0, \tag{10}$$

The field in the grating is a combination of the two waves $R(x)$ and $S(x)$. At the upper frequency of the stopband [20],

$$R(x) + S(x) = 2(c_1 + c_2) \cos\left(k_0 x - \frac{\varphi_k}{2}\right) \exp\left(-i\frac{\varphi_k}{2}\right), \tag{11}$$

at the lower frequency,

$$R(x) + S(x) = 2(c_1 + c_2) \sin\left(k_0 x - \frac{\varphi_k}{2}\right) \exp\left[-i\left(\frac{\varphi_k}{2} + \frac{\pi}{2}\right)\right], \tag{12}$$

After finding the positions of the nodes of the standing wave during the frequencies at the stopband edges, one can get the phase of κ. In an open-circuited grating, the current density $\partial I/\partial x$ is equal to zero, this yields the following equation

$$V = \frac{2\alpha^*}{\omega C} R(x) + \frac{2\alpha}{\omega C} S(x), \tag{13}$$

Substituting Equation (13) into the remaining COM equations, we have

$$\begin{cases} \dfrac{\partial R_0}{\partial x} = -i\left(\Delta - \dfrac{2|\alpha|^2}{\omega C}\right) R_0(x) + i\left(\kappa + \dfrac{2\alpha^2}{\omega C}\right) S_0(x) \\ \dfrac{\partial S_0}{\partial x} = -i\left(\kappa^* + \dfrac{2(\alpha^*)^2}{\omega C}\right) R_0(x) + i\left(\Delta - \dfrac{2|\alpha|^2}{\omega C}\right) S_0(x) \end{cases}, \tag{14}$$

The general solutions of Equation (14) are the same as Equation (4), but with the corresponding equivalent detuning parameter $\Delta_{oc} = \Delta - 2|\alpha|^2/(\omega C)$ and the equivalent reflection coefficient $\kappa_{oc} = \kappa + 2\alpha^2/(\omega C)$. The dispersion relation should be modified by Δ_{oc} and κ_{oc}. We also use the phase φ_α and amplitude $|\alpha|$ to describe the transduction

coefficient as $\alpha = |\alpha| \exp(i\varphi_\alpha)$. The upper and lower frequencies of the stopband f_{o+} and f_{o-} in an open-circuited grating can be expressed considering Equation (7) as:

$$\begin{cases} f_{o+} = \left(1 + \frac{\lambda_0}{2\pi} \frac{2|\alpha|^2}{\omega C} + \frac{\lambda_0}{2\pi} \left| \kappa + \frac{2\alpha^2}{\omega C} \right| \right) f_s \\ f_{o-} = \left(1 + \frac{\lambda_0}{2\pi} \frac{2|\alpha|^2}{\omega C} - \frac{\lambda_0}{2\pi} \left| \kappa + \frac{2\alpha^2}{\omega C} \right| \right) f_s \end{cases}, \tag{15}$$

The amplitude of a regeneration reflection term $2|\alpha|^2/(\omega C)$ can be obtained by Equation (16)

$$\frac{2|\alpha|^2}{\omega C} = \frac{2\pi}{\lambda_0} \left(\frac{f_{o+} + f_{o-}}{f_{s+} + f_{s-}} - 1 \right), \tag{16}$$

Moreover, we will get the amplitude of the reflection coefficient in an open-circuited grating:

$$\left| \kappa + \frac{2\alpha^2}{\omega C} \right| = \frac{2\pi}{\lambda_0} \frac{f_{o+} - f_{o-}}{f_{s+} + f_{s-}}, \tag{17}$$

According to the method mentioned above, we can obtain the phase of the reflection coefficient in an open-circuited grating $\varphi_{\kappa o}$. Making full use of Equations (9), (16) and (17), and the phase of φ_κ and $\varphi_{\kappa o}$, we can get

$$\begin{cases} \cos(2\varphi_\alpha) = \dfrac{\left| \kappa + \frac{2\alpha^2}{\omega C} \right| \cos(\varphi_{\kappa o}) - |\kappa| \cos(\varphi_\kappa)}{\frac{2|\alpha|^2}{\omega C}} \\ \sin(2\varphi_\alpha) = \dfrac{\left| \kappa + \frac{2\alpha^2}{\omega C} \right| \sin(\varphi_{\kappa o}) - |\kappa| \sin(\varphi_\kappa)}{\frac{2|\alpha|^2}{\omega C}} \end{cases}, \tag{18}$$

So far, we have solved the four COM parameters including the phases of κ and α. We can get another relation from the edge frequencies of the stopband in a short-circuited grating and an open-circuited grating

$$\cos(\varphi_\kappa - 2\varphi_\alpha) = \frac{(f_{o+} - f_{o-})^2 - (f_{s+} - f_{s-})^2 - (f_{o+} + f_{o-} - f_{s+} - f_{s-})^2}{2(f_{s+} - f_{s-})(f_{o+} + f_{o-} - f_{s+} - f_{s-})}, \tag{19}$$

The Equation (19) is similar to (7.154) of reference [18], and it can be used to verify the phase difference between the phase φ_κ and the double phase φ_α.

2.3. FEM Model Description and Simulation

The wave of the Rayleigh-type SAW propagates on the surface of the substrate with its amplitude exponentially decaying. This feature enables us to build a model with only a few wavelength depths of the substrate. The waves, excited by infinite numbers of the IDT fingers with the same grating shape on a piezoelectric substrate, are spatially periodic. Therefore, simulating a periodic structure of the device might suffice. With the use of periodic boundary conditions (PBC) in x- and y-directions, this model is reduced to one period λ_0 in the x-direction and $\lambda_0/10$ in the y-direction. Static analysis and eigenfrequency analysis are conducted in the FEM to extract the COM parameters. Here, we build the FEM model of a standard EWC SPUDT cell on a substrate to demonstrate the approach to extract the COM parameters.

As shown in Figure 2, a three-dimensional model with a period of λ_0 = 50 μm, in which the IDT structure is a standard EWC SPUDT, is built. This standard EWC SPUDT has three fingers, with two $\lambda_0/8$ narrow fingers and one $\lambda_0/4$ wide finger, and the gaps

between the fingers are $\lambda_0/8$ and $3\lambda_0/16$. The first finger is active. In our model, we set the origin at the center of the period structure. A perfectly matched layer (PML) is applied to suppress the spurious resonances caused by the bottom reflection [30]. The thickness of electrodes is denoted by h and the thickness of the substrate and the PML are set as $5\lambda_0$ and λ_0, respectively. Two electrodes on the right in the model are grounded, while the terminal one is 1V voltage or 0C charge, according to the request of the model analysis.

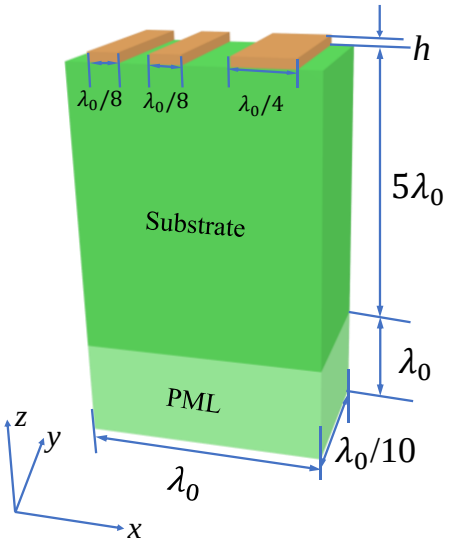

Figure 2. FEM model of a unit cell.

In Equation (3), the COM parameters can be interpreted as parameters for a unit length. Actually, the parameters for a unit period of length λ_0 are more practical. Instead, it is convenient to define the normalized parameters listed in Table 1.

In static analysis, a voltage 1V is applied on the terminal electrode. After the model is solved, we can get the surface charge density $\sigma_s(x_1)$ and the tangential component of the electric field on the substrate surface $E_1(x_1)$ and the surface potential $\Phi(x_1)$, as shown in Figure 3.

The capacitance can be calculated by summing the electrostatic charges on the electrodes connected to the terminal of voltage.

The other COM parameters can be obtained from the results of the eigenfrequency analysis. In this analysis, the edge frequencies of the stopband $f_{s+}, f_{s-}, f_{o+}, f_{o-}$ can be obtained. The two frequencies (f_{s+} and f_{s-}) correspond to two eigenfrequencies (symmetric frequency and antisymmetric frequency) of the eigenfrequency analysis by setting the terminal voltage to 0V. Here, we also donate the lower of the two eigenfrequencies as f_{s-} and the higher one as f_{s+}, and they are 77.646 MHz and 78.079 MHz for 128° YX $LiNbO_3$, respectively. The displacement distributions at the lower and upper stopband edges also can be obtained from the postprocessing of the eigenfrequency analysis in the FEM, and the normalized displacements are shown in Figure 4.

Table 1. Normalized COM parameters.

Parameters	Symbol	Dimension (SI)
Velocity in short-circuited grating	v	m/s
Reflection coefficient	$\kappa_p = \kappa\lambda_0$	%
Transduction coefficient	$\alpha_p = \alpha\lambda_0$	$\Omega^{-\frac{1}{2}}$
Normalized transduction coefficient α_n	$\alpha_p/\sqrt{\omega C_p}$	%
Capacitance	$C_p = C\lambda_0$	F
Normalized capacitance	$C_n = C_p/W$	F/m

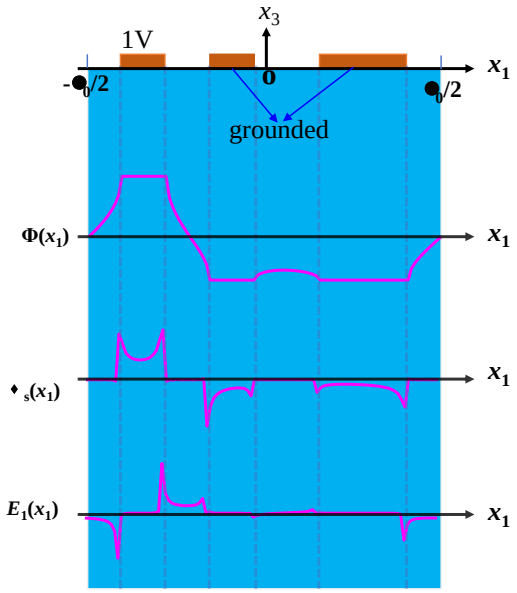

Figure 3. Surface potential, surface charge density and tangential component of the electric field distribution under a periodic EWC SPUDT.

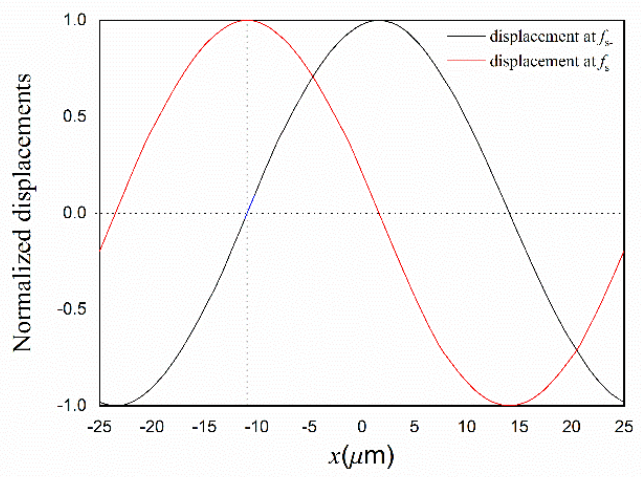

Figure 4. Normalized displacement distributions at the lower and upper edge frequencies.

It can be seen that there is a $\pi/2$ phase difference between the two displacements distribution. One can get the phase φ_κ after finding the position of the displacement distribution at the lower edge frequency. Then, the COM parameters of ν, $|\kappa|$ and φ_κ can be derived using Equations (8)–(12). Table 2 gives the calculated COM parameters for EWC SPUDT on 128°YX $LiNbO_3$ with h = 0.

Table 2. COM parameters for EWC SPUDT on 128°YX $LiNbO_3$ for h = 0.

Parameters	Values
Normalized capacitance (pF/m)	546.33
Velocity in short-circuited grating (m/s)	3892.7
Reflection coefficient $\lvert\kappa_p\rvert$ (%)	1.73
Phase of reflection coefficient	−157.56°
Normalized transduction coefficient α_n (%)	14.68
Phase of transduction coefficient	−37.84°

We have extracted the COM parameters [31] for EWC SPUDT on YZ-$LiNbO_3$, bidirectional IDTs on 128°YX $LiNbO_3$ and Y-Z $LiNbO_3$. Moreover, these results are compared with those of well-known researchers in the field of surface acoustic waves (SAW), and that shows this approach is powerful to fully extract the COM parameters of the Rayleigh-type SAW for all kinds of IDT structures on arbitrary materials [20,32,33].

We modify the directivity D given in reference [18], which can be simplified to Equation (20):

$$D = \left| \frac{1 + i\exp(i\varphi)\tanh\left(\frac{N|\kappa_p|}{2}\right)}{1 + i\exp(-i\varphi)\tanh\left(\frac{N|\kappa_p|}{2}\right)} \right|, \tag{20}$$

where $\varphi = \varphi_\kappa - 2\varphi_\alpha$, we call it unidirectional angle, and N is the number of electrodes.

In Equation (20), the defined directivity is the ratio of the excitation efficiency of the IDT in positive x to the excitation efficiency in negative x. This means that the wave excitation in direction of positive x is favored over the negative x if $D > 1$, and the wave excitation in positive x is weaker than the negative x if $D < 1$, or else the period of an IDT cell on a given substrate is bidirectional. When fixed for the value $N|\kappa_p|$, one can find that the condition of the best right directivity is $\varphi = -\pi/2$. The sign of φ is important to decide the direction of the wave excited by the drive voltage is applied on IDTs. Definitely, one can get the sign of φ since all the COM parameters, including the phases of φ_κ and φ_α, can be calculated by our method.

3. Results and Discussions

In this section, we compute the COM parameters versus the thickness of the electrode for the bidirectional IDT on the 128°YX $LiNbO_3$, bidirectional IDT on Y-Z $LiNbO_3$, EWC SPUDT on 128°YX $LiNbO_3$ and EWC on Y-Z $LiNbO_3$, respectively. The material constants of $LiNbO_3$ are obtained from reference [34], and the metal electrodes are assigned with aluminum (Al) material with a Young's modulus of 70 GPa, a Poisson's ratio of 0.33 and a density of 2700 kg/m^3.

Figure 5a–d illustrates the results of the COM parameters for the bidirectional IDT on the 128°YX $LiNbO_3$. As shown in Figure 5a, with an increase of h/λ_0, the velocity v decreases, while the capacitance C_n has almost no change. Figure 5b shows the amplitude and the phase of κ. It is easy to see that $|\kappa|$ decreases at first and then increases with the increase of h/λ_0, and it becomes zero at $h/\lambda_0 \approx 2.76\%$. This is due to the fact that the electrical reflection by the short-circuited grating has the opposite sign to the mechanical reflection [18]. The corresponding experiment results [35] verified its correctness. This phenomenon can be deduced from the phase φ_κ. When h/λ_0 is small, $\varphi_\kappa = \pi$, namely, $\kappa < 0$, and when $h/\lambda_0 > 2.76\%$, $\varphi_\kappa = 0$, namely, $\kappa > 0$. This is to say that κ increases monotonically with an increase in h/λ_0. Figure 5c shows α_n and the phase φ_α. We can see that the value of α_n has a slowly increasing trend and that the phase remains the same at zero. The directivity and the unidirectional angle versus the thickness of the electrode are displayed in Figure 5d. It can be seen that the directivity has stayed at 1, indicating that the IDT is bidirectional and there is no natural unidirectionality in the material orientation. In Figure 5d, we can see the unidirectional angle is 0 or 180°. Substituting the unidirectional angle into Equation (20), the directivity of 1 also can be deduced.

Figure 6a–d illustrate the results of the COM parameters for the bidirectional IDT on the Y-Z $LiNbO_3$. The COM parameters of C and v have the same change trends compared with the bidirectional IDT on 128°YX-$LiNbO_3$, while the value of α_n has an opposite trend. From Figure 6b, the reflection coefficient increases without an inflection point and the phase φ_κ is offset by 0 slightly and increases slowly with h/λ_0. These features demonstrate that directivity is inherent in Y-Z $LiNbO_3$ despite being very small. Additionally, the directivity can be adjusted slightly by changing the thickness of the electrode. It also can be seen

from Figure 6d that the unidirectional angle is offset by 180° when h/λ_0 increases, and the directivity increases as h/λ_0 increases.

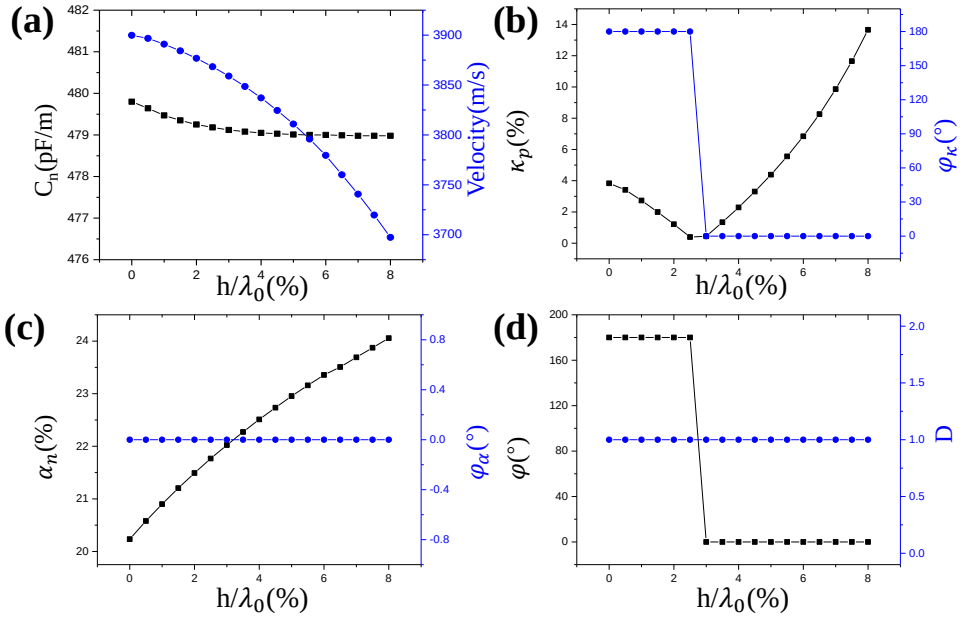

Figure 5. COM parameters versus thickness of electrode for bidirectional IDT on 128°YX $LiNbO_3$: (**a**) Normalized capacitance and velocity; (**b**) Reflection coefficient and its phase; (**c**) Normalized transduction coefficient and its phase; (**d**) The unidirectional angle and directivity.

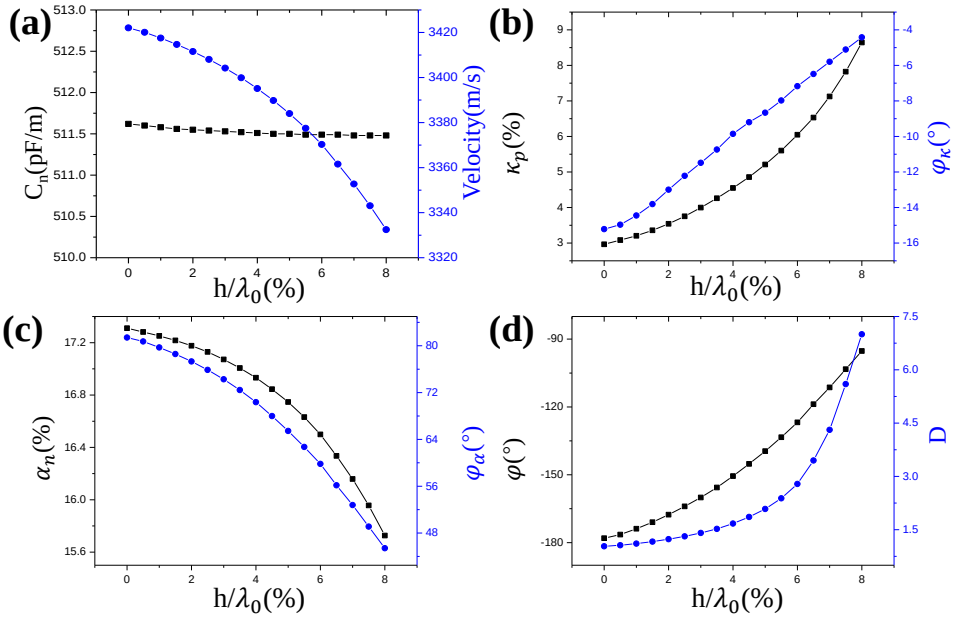

Figure 6. COM parameters versus thickness of electrode for bidirectional IDT on YZ-$LiNbO_3$: (**a**) Normalized capacitance and velocity; (**b**) Reflection coefficient and its phase; (**c**) Normalized transduction coefficient and its phase; (**d**) The unidirectional angle and directivity.

Figures 7a–d and 8a–d illustrate the results of the COM parameters for the EWC SPUDT on 128°YX LiNbO3 and Y-Z $LiNbO_3$, respectively. These COM parameters of C, ν and α_n have the same change trends in two cutting types of $LiNbO_3$. The same is seen in the bidirectional IDT, where the $|\kappa_p|$ has a zero [36] value in 128°YX-$LiNbO_3$ when h/λ_0 is approximate to 2.47%, but such a zero value does not exist in YZ-$LiNbO_3$. In relation to the

$|\kappa_p|$, it is relatively small in the EWC SPUDT structure compared with the bidirectional IDT structure. From Figures 7d and 8d, we can see that the unidirectional angles are close to $-90°$ or $90°$, but not $-90°$ or $90°$ exactly. This means that the standard EWC SPUDT structure on 128°YX $LiNbO_3$ and Y-Z $LiNbO_3$ do not obtain the best directivity. From the directivity curve in Figure 7d, the wave excitation in the right direction is favored over the left wave when h/λ_0 is small, while when h/λ_0 is larger than 2.76%, this is reversed. This phenomenon has not appeared in previous research and is not found in YZ-$LiNbO_3$.

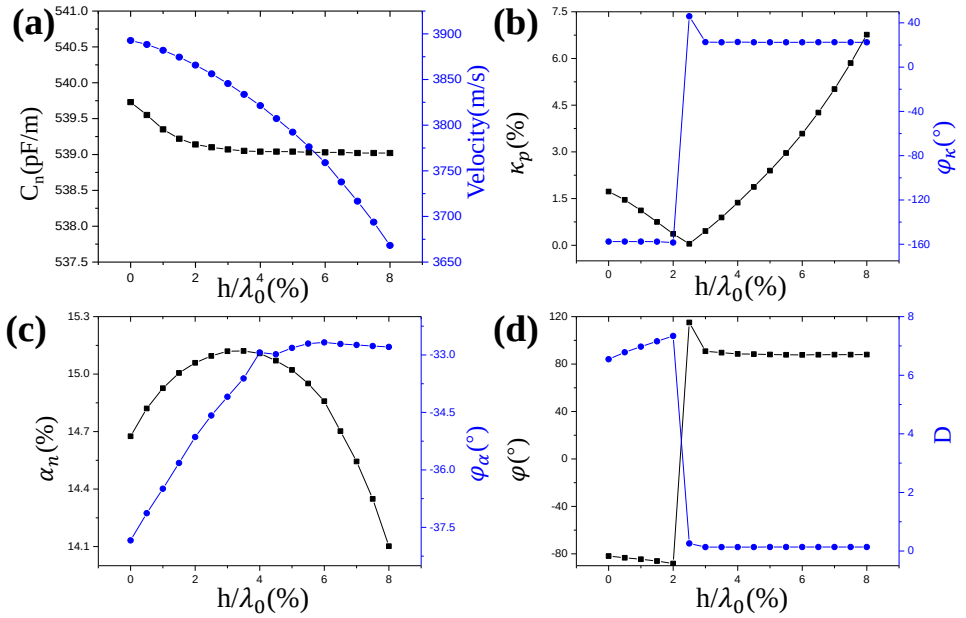

Figure 7. COM parameters versus thickness of electrode for EWC SPUDT on 128°YX-$LiNbO_3$: (**a**) Normalized capacitance and velocity; (**b**) Reflection coefficient and its phase; (**c**) Normalized transduction coefficient and its phase; (**d**) The unidirectional angle and directivity.

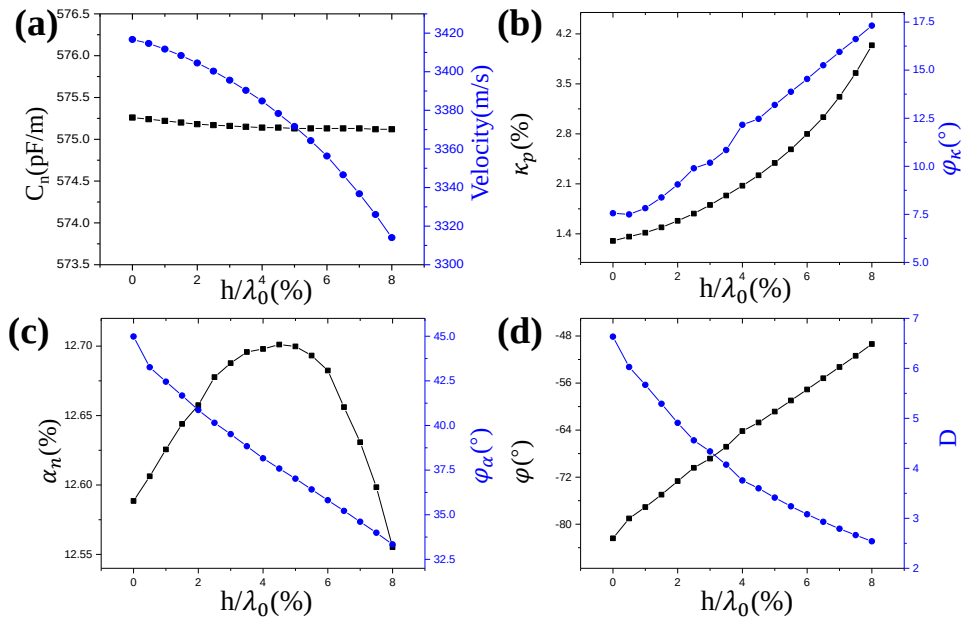

Figure 8. COM parameters versus thickness of electrode for EWC SPUDT on YZ-$LiNbO_3$: (**a**) Normalized capacitance and velocity; (**b**) Reflection coefficient and its phase; (**c**) Normalized transduction coefficient and its phase; (**d**) The unidirectional angle and directivity.

4. Conclusions

A novel method is proposed to extract all the COM parameters, especially for the phases φ_κ and φ_α. This method fully utilizes the static and eigenfrequency characteristics computed by the FEM. The corresponding relationships between the characteristics obtained by the FEM and the characteristics in the COM theory are established. All the COM parameters for a bidirectional IDT cell on 128°YX $LiNbO_3$, a bidirectional IDT cell on Y-Z $LiNbO_3$, an EWC SPUDT cell on 128°YX $LiNbO_3$ and an EWC SPUDT cell on Y-Z $LiNbO_3$ are calculated, respectively. These examples show that this is an effective method to extract the COM parameters quickly, accurately, generally and fully.

Author Contributions: Conceptualization, X.S. (Xueping Sun), W.W. and W.L.; methodology, X.S. (Xueping Sun); software, X.S. (Xueping Sun) and R.M.; validation, X.S. (Xiuting Shao), W.W. and S.Z.; formal analysis, D.L.; investigation, X.S. (Xueping Sun); resources, W.W.; data curation, X.S. (Xueping Sun) and R.M.; writing—original draft preparation, X.S. (Xueping Sun); writing—review and editing, X.S. (Xueping Sun); visualization, X.S. (Xiuting Shao) and D.L.; supervision, W.W. and W.L.; project administration, W.L.; funding acquisition, J.C., X.S. (Xiuting Shao) and S.Z. All authors have read and agreed to the published version of the manuscript.

Funding: This research was funded by the Natural Science Basic Research Program of Shaanxi, grant number 2022JQ-676, and the Scientific Research Program of Shaanxi Provincial Education Department, grant number 21JY017, and the National Natural Science Foundation of China, grant number 11804201.

Institutional Review Board Statement: Not applicable.

Informed Consent Statement: Not applicable.

Data Availability Statement: Not applicable.

Conflicts of Interest: The authors declare no conflict of interest.

References

1. Belyankova, T.; Vorovich, E.; Kalinchuk, V.; Tukodova, O. Specific features of SH-waves propagation in structures with prestressed inhomogeneous coating made of piezoceramics based on LiNbO 3. *J. Adv. Dielectr.* **2021**, *11*, 2160007. [CrossRef]
2. Belyankova, T.; Vorovich, E.; Kalinchuk, V.; Tukodova, O. Peculiarities of surface acoustic waves, propagation in structures with functionally graded piezoelectric materials, coating from different ceramics on the basis of PZT. *J. Adv. Dielectr.* **2020**, *10*, 2060017. [CrossRef]
3. Hofer, M.; Finger, N.; Kovacs, G.; Schoberl, J.; Zaglmayr, S.; Langer, U.; Lerch, R. Finite-element simulation of wave propagation in periodic piezoelectric SAW structures. *IEEE Trans. Ultrason. Ferroelectr. Freq. Control* **2006**, *53*, 1192–1201. [CrossRef] [PubMed]
4. Koskela, J.; Plessky, V.; Willemsen, B.; Turner, P.; Hammond, B.; Fenzi, N. Hierarchical cascading algorithm for 2-D FEM simulation of finite SAW devices. *IEEE Trans. Ultrason. Ferroelectr. Freq. Control* **2018**, *65*, 1933–1942. [CrossRef] [PubMed]
5. Willemsen, B.; Plesski, V.; Koskela, J. Fast, Highly Accurate, Full-Fem Surface Acoustic Wave Simulation. U.S. Patent 11,296,677, 5 April 2022.
6. Li, X.; Bao, J.; Huang, Y.; Zhang, B.; Omori, T.; Hashimoto, K.-Y. Use of Hierarchical Cascading Technique for FEM Analysis of Transverse-Mode Behaviors in Surface Acoustic-Wave Devices. *IEEE Trans. Ultrason. Ferroelectr. Freq. Control* **2019**, *66*, 1920–1926. [CrossRef]
7. Li, X.; Bao, J.; Qiu, L.; Matsuoka, N.; Omori, T.; Hashimoto, K.-Y. 3D FEM simulation of SAW resonators using hierarchical cascading technique and general purpose graphic processing unit. *Jpn. J. Appl. Phys.* **2019**, *58*, SGGC05. [CrossRef]
8. Fernandez-Afonso, Y.; García-Zaldívar, O.; Calderón-Piñar, F. Equivalent circuit for the characterization of the resonance mode in piezoelectric systems. *J. Adv. Dielectr.* **2015**, *5*, 1550032. [CrossRef]
9. Plessky, V.; Koskela, J. Coupling-of-modes analysis of SAW devices. *Int. J. High Speed Electron. Syst.* **2000**, *10*, 867–947. [CrossRef]
10. Hartmann, C.; Abbott, B. Experimentally determining the transduction magnitude and phase and the reflection magnitude and phase of SAW SPUDT structures. In Proceedings of the IEEE Symposium on Ultrasonics, Honolulu, HI, USA, 4–7 December 1990; pp. 37–42.
11. Kondratiev, S.; Thorvaldsson, T.; Sakharov, S.; Buzanov, O.; Medvedev, A. Extraction of COM parameters on langasite substrates and the application to design of a SAW filter. In Proceedings of the 2001 IEEE Ultrasonics Symposium. Proceedings. An International Symposium (Cat. No. 01CH37263), Atlanta, GA, USA, 7–10 October 2001; pp. 53–56.
12. Ventura, P.; Hodé, J.; Solal, M.; Desbois, J.; Ribbe, J. Numerical methods for SAW propagation characterization. In Proceedings of the 1998 IEEE Ultrasonics Symposium. Proceedings (Cat. No. 98CH36102), Sendai, Japan, 5–8 October 1998; pp. 175–186.

13. Dufilie, P.; Ventura, P.; Hecht, F. COM parameters for thick metal and partially buried electrodes extracted from a mixed FEM/BEM numerical model. In Proceedings of the 2012 IEEE International Ultrasonics Symposium, Dresden, Germany, 7–10 October 2012; pp. 807–810.
14. Shaposhnikov, K.; Kaltenbacher, M.; Nicolay, P. Fast full-FEM computation of COM parameters. Application to multilayered SAW structures. In Proceedings of the 2014 IEEE International Ultrasonics Symposium, Chicago, IL, USA, 3–6 September 2014; pp. 1501–1504.
15. Hashimoto, K.-Y.; Zheng, G.Q.; Yamaguchi, M. Fast analysis of SAW propagation under multi-electrode-type gratings with finite thickness. In Proceedings of the 1997 IEEE Ultrasonics Symposium Proceedings. An International Symposium (Cat. No. 97CH36118), Toronto, ON, Canada, 5–8 October 1997; pp. 279–284.
16. Hashimoto, K.-Y.; Koskela, J.; Salomaa, M.M. Fast determination of coupling-of-modes parameters based on strip admittance approach. In Proceedings of the 1999 IEEE Ultrasonics Symposium. Proceedings. International Symposium (Cat. No. 99CH37027), Tahoe, NV, USA, 17–20 October 1999; pp. 93–96.
17. Hartmann, C.; Wright, P.; Kansy, R.; Garber, E. An analysis of SAW interdigital transducers with internal reflections and the application to the design of single-phase unidirectional transducers. In Proceedings of the 1982 Ultrasonics Symposium, San Diego, CA, USA, 27–29 October 1982; pp. 40–45.
18. Hashimoto, K.-y.; Hashimoto, K.-Y. *Surface Acoustic Wave Devices in Telecommunications*; Springer: Berlin/Heidelberg, Germany, 2000; Volume 116.
19. Ruppel, C.C.; Fjeldly, T.A. *Advances in Surface Acoustic Wave Technology, Systems and Applications*; World Scientific: Singapore, 2001; Volume 20.
20. Lin, J.; Wang, N.; Chen, H.; Shui, Y. Fast, precise, and full extraction of the COM parameters for multielectrode-type gratings by periodic Green's function method. *IEEE Trans. Ultrason. Ferroelectr. Freq. Control* **2002**, *49*, 1735–1738.
21. Chen, D.-P.; Haus, H.A. Analysis of metal-strip SAW gratings and transducers. *IEEE Trans. Sonics Ultrason.* **1985**, *32*, 395–408. [CrossRef]
22. Hashimoto, K.-y.; Omori, T.; Ahn, C.-J. Extension of scalar potential formalism for transverse mode analysis of surface acoustic wave resonators. In Proceedings of the 2011 IEEE International Ultrasonics Symposium, Orlando, FL, USA, 18–21 October 2011; pp. 333–336.
23. Huang, Y.; Bao, J.; Li, X.; Zhang, B.; Omori, T.; Hashimoto, K.-Y. Parameter extraction of coupling-of-modes equations including coupling between two surface acoustic waves on SiO_2/Cu/$LiNbO_3$ structures. *Jpn. J. Appl. Phys.* **2018**, *57*, 07LD13. [CrossRef]
24. Abbott, B.P. *A Coupling-of-Modes Model for SAW Transducers with Arbitrary Reflectivity Weighting*; University of Central Florida: Orlando, FL, USA, 1989.
25. Wu, T.-T.; Wang, S.-M.; Chen, Y.-Y.; Wu, T.-Y.; Chang, P.-Z.; Huang, L.-S.; Wang, C.-L.; Wu, C.-W.; Lee, C.-K. Inverse determination of coupling of modes parameters of surface acoustic wave resonators. *Jpn. J. Appl. Phys.* **2002**, *41*, 6610. [CrossRef]
26. Chen, Y.-Y.; Wu, T.-T.; Chou, T.-T. Analysis of the frequency response of a dispersive IDT/ZnO/sapphire SAW filter using effective permittivity and the coupling of modes model. *J. Phys. D Appl. Phys.* **2003**, *37*, 120. [CrossRef]
27. Alyakna, Y.Y.; Gulyaev, Y.V.; Kozlov, A.; PLESSKII, V. Infulence of modulation of the grrove depth of a Bragg reflective grating on the Rayleigh-wave reflection coefficient. *Sov. Phys. Acoust.-USSR* **1984**, *30*, 346–348.
28. Sun, X.; Liu, W.; Ge, S.; Zhou, S.; Li, X.; Lin, D. Achieving both high electromechanical response and stable temperature behavior in Si/SiO_2/Al/$LiTaO_3$ sandwich structure. *AIP Adv.* **2019**, *9*, 035145. [CrossRef]
29. Zhang, Y.-m.; Jin, J.; Li, H.-l.; Hu, H.-p. A novel method to extract COM parameters for SAW based on FEM. In Proceedings of the 2019 13th Symposium on Piezoelectrcity, Acoustic Waves and Device Applications (SPAWDA), Harbin, China, 11–14 January 2019; pp. 1–5.
30. Dühring, M.B.; Laude, V.; Khelif, A. Energy storage and dispersion of surface acoustic waves trapped in a periodic array of mechanical resonators. *J. Appl. Phys.* **2009**, *105*, 093504. [CrossRef]
31. Sun, X.; Zhou, S.; Cheng, J.; Lin, D.; Liu, W. Full extraction of the COM parameters for Rayleigh type surface acoustic wave. *AIP Adv.* **2022**, *12*, 025007. [CrossRef]
32. Koskela, J.; Plessky, V.P.; Salomaa, M.M. SAW/LSAW COM parameter extraction from computer experiments with harmonic admittance of a periodic array of electrodes. *IEEE Trans. Ultrason. Ferroelectr. Freq. Control* **1999**, *46*, 806–816. [CrossRef]
33. Lin, J.; Wu, H.; Wang, N.; Qiu, H.; Shui, Y.A. Precise and full extraction of the coupling-of-mode parameters with periodic Green's function. *Sci. China Ser. F Inf. Sci.* **2003**, *46*, 298–308. [CrossRef]
34. Kovacs, G.; Anhorn, M.; Engan, H.; Visintini, G.; Ruppel, C. Improved material constants for LiNbO/sub 3/and LiTaO/sub 3. In Proceedings of the IEEE symposium on ultrasonics, Honolulu, HI, USA, 4–7 December 1990; pp. 435–438.
35. He, S.; Chen, D.; Wang, C. The Structures of SAW Single-electrode IDT without Internal Reflection and the Analysis on Their Properties. *Piezoelectr. Acoustoopt.* **1992**, *14*, 55–59. (In Chinese)
36. Sun, X.; Liu, W.; Shao, X.; Zhou, S.; Wang, W.; Lin, D. Surface acoustic wave gyroscopic effect in an interdigital transducer. *Sensors* **2018**, *19*, 106. [CrossRef] [PubMed]